Computational-Experimental Study of the Onset Potentials for CO2 reduction on Polycrystalline and Oxide-Derived Copper Electrodes

Article *in* Electrochimica Acta · March 2021

DOI: 10.1016/j.electacta.2021.138247

4 authors, including:

Oriol Piqué
University of Barcelona
13 PUBLICATIONS **186** CITATIONS
SEE PROFILE

Mario Löffler
Forschungszentrum Jülich
19 PUBLICATIONS **220** CITATIONS
SEE PROFILE

Ioannis Katsounaros
Forschungszentrum Jülich
102 PUBLICATIONS **5,241** CITATIONS
SEE PROFILE

Electrochimica Acta 380 (2021) 138247

Contents lists available at ScienceDirect

Electrochimica Acta

journal homepage: www.elsevier.com/locate/electacta

Computational-experimental study of the onset potentials for CO_2 reduction on polycrystalline and oxide-derived copper electrodes

Oriol Piqué [a], Mario Löffler [b,c], Ioannis Katsounaros [b,*], Federico Calle-Vallejo [a,*]

[a] Department of Materials Science and Physical Chemistry & Institute of Theoretical and Computational Chemistry (IQTCUB), University of Barcelona, Martí i Franquès 1, 08028 Barcelona, Spain
[b] Helmholtz Institute Erlangen-Nürnberg for Renewable Energy (IEK-11), Forschungszentrum Jülich GmbH, Egerlandstr. 3, 91058 Erlangen, Germany
[c] Department of Chemical and Biological Engineering, Friedrich-Alexander-Universität Erlangen-Nürnberg (FAU), Egerlandstr. 3, 91058 Erlangen, Germany

ARTICLE INFO

Article history:
Received 11 December 2020
Revised 8 February 2021
Accepted 20 March 2021
Available online 26 March 2021

Keywords:
CO_2 electroreduction
onset potential
polycrystalline Cu
Oxide-derived Cu
DFT
Real time quantification

ABSTRACT

The electrocatalytic reduction of CO_2 (CO_2RR) is a promising yet intricate process to alleviate the alarming imbalance in the carbon cycle. One of the intricacies of CO_2RR is its structural sensitivity, which is illustrated by the varying onset potentials and selectivities of the reaction products depending on the electrode morphology. Here, using electrochemical real-time mass spectrometry (EC-RTMS), we accurately determine the onset potentials for seven CO_2RR products including C_1, C_2, and C_3 species on polycrystalline and oxide-derived Cu electrodes. Density functional theory calculations affordably including solvent and cation effects produce onset potentials of C_2 species matching those obtained with EC-RTMS. Our analysis leads us to conclude that the elusive active sites at oxide-derived Cu, known to enhance ethanol production, are undercoordinated square ensembles of Cu atoms.

1. Introduction

Powered by renewable electricity, the electrochemical reduction of CO_2 (CO_2RR) is a plausible approach to help compensate the tremendous global imbalance of the carbon cycle. In doing so, the alarming amounts of CO_2 in the environment can be transformed into valuable chemical compounds such as methane, ethanol and ethylene [1–3]. As shown by the pioneering works of Hori et al., copper is capable of reducing CO_2 beyond the two-electron products (CO or formic acid) observed on most metals [4–6]. However, the predominance of the competing hydrogen evolution, the low selectivity toward specific products, and the large overpotentials needed to obtain fair current densities still hinder a large-scale implementation of Cu-based CO_2 electrolyzers. Interestingly, the redox treatment of Cu electrodes holds promise for addressing some of these issues [7,8].

In fact, oxide-derived copper (OD-Cu) electrocatalysts show lower overpotentials and enhanced selectivity toward C_2 products, with higher faradaic efficiencies of ethanol compared to regular Cu electrodes [7,8]. In spite of some hints, the active sites responsible for such improvements have not been ascertained yet in experiments. For instance, it is known that the presence and extent of grain boundaries are connected with the activity improvements of OD-Cu [7,9]. Furthermore, isotopic labelling experiments of CO_2RR on OD-Cu showed that ethylene and ethanol, the two major C_2 products, are produced on different active sites [10]. On the other hand, ethylene is more abundant than ethanol on pristine Cu(100) facets [11], while increasing amounts of ethanol are observed at rough Cu surfaces.

The recent development of the electrochemical real-time mass spectrometry technique (EC-RTMS) allows for accurate, *in operando* detection of CO_2RR products on OD-Cu and polycrystalline Cu (Cu-poly) [12,13]. The sensitivity of this real-time technique for reaction products and intermediates is remarkably high compared to established chromatography techniques or nuclear magnetic resonance, which are compatible with steady-state electrolysis [13]. The low limits of detection enable a more accurate determination of onset potentials based on the detection of products at low formation rates during potential sweep experiments. This is rather useful for CO_2RR, as different compounds are produced as a function of the applied potential and, in some cases, some products appear at similar if not identical potentials.

Furthermore, computational studies have shown that solvation and cation effects are key to accurately predict the CO_2RR activity and selectivity of Cu electrodes [1,14–18]. Remarkably, several experimental investigations have shown that alkaline cations enhance the production of multi-carbon species [19–22]. Different

* Corresponding authors.
E-mail addresses: i.katsounaros@fz-juelich.de (I. Katsounaros), f.calle.vallejo@ub.edu (F. Calle-Vallejo).

https://doi.org/10.1016/j.electacta.2021.138247
0013-4686/

approaches have been used to model these effects. Using static calculations, solvation can be modelled using implicit solvent models [23], ad hoc corrections [14,24,25], explicit water layers [17,26], or using micro-solvation models in which explicit water molecules are added in the vicinity of the adsorbates to capture their hydrogen bonds [27,28]. On the other hand, (solvated) cations can be modelled through an electric field [29], by including them within an explicit water bilayer [26,30], by adsorbing them next to the adsorbates [16,22,31], or by means of continuum models of the double-layer [32]. Specific choices for the modelling of these effects depend on the system size and complexity, usually attempting to compromise computational expenses and accuracy.

In this work, we provide the onset potentials for seven CO_2RR products including C_1, C_2, and C_3 species using EC-RTMS experiments. In addition, we show that calculations affordably including solvent and cation effects produce onset potentials of C_2 species matching those obtained experimentally with EC-RTMS. This helps in outlining a plausible geometric structure of the active sites at OD-Cu and leads to interesting mechanistic conclusions.

2. Methods

2.1. Experimental details

Details on the analysis of gaseous and liquid products with electrochemical real-time mass spectrometry (EC-RTMS) have been described previously [13,33]. Linear sweep voltammetry at a scan rate of 3 mV s^{-1} was conducted from −0.4 to −1.1 V_{RHE} for Cu-poly and from −0.1 to −0.8 V_{RHE} for OD-Cu, always in the negative direction of the potential (V_{RHE} denotes potentials in the reversible hydrogen electrode scale). The starting potentials were such that neither CO_2 reduction nor extensive hydrogen evolution takes place, while the surface oxidation state remains unaltered until the measurement starts. Parallel to the electrochemical data of current and potential versus time, information on the formed products was obtained versus time as well, with a data acquisition frequency of ca. 1.7 Hz for the gas analysis and 2 Hz for the liquid analysis. The mass spectrometric data were synchronized with the electrochemical data after the measurement, taking into account the time needed for the formed products to reach the corresponding mass spectrometer, and eventually the intensities for each product were expressed as a function of the applied potential after post-correction for the remaining 36–41 Ω after 85% positive feedback compensation. The evaluation procedure to determine the onset potential of each product from the respective mass spectrometry signals is described in section S1 of the Supporting Information (SI).

For the preparation of Cu-poly and OD-Cu electrodes, we employed the same procedure described in a previous work [13]. The thermally oxidized electrodes were reduced electrochemically at −1.2 V_{RHE} for 10 min before the linear sweep voltammetry was applied, to make sure that the oxide reduction did not interfere with the product evolution during the linear sweep. Ultrapure water (18.2 MΩ cm, TOC <5 ppb, Merck Milli-Q IQ 7000) was used for the preparation of the electrolyte, right before each measurement. For the CO_2 reduction experiments, the electrolyte was 0.1 M $KHCO_3$ (analysis grade, Merck) saturated in CO_2 (99.998%, Air Liquide) and the resulting pH of the solution was 6.8. For the acetaldehyde reduction experiments, the electrolyte was 0.05 M Na_2HPO_4 (99%, VWR), 0.05 M $NaH_2PO_4 \cdot 2H_2O$ (99%, VWR) (pH set to 6.8 equal to the pH of 0.1 M $KHCO_3$ saturated in CO_2) and 1 mM acetaldehyde (≥99.0%, VWR) saturated in Argon (99.998%, Air Liquide). In either case, the electrolyte was sparged with the respective gas for 30 min before the measurement started, and sparging was maintained throughout the entire measurement.

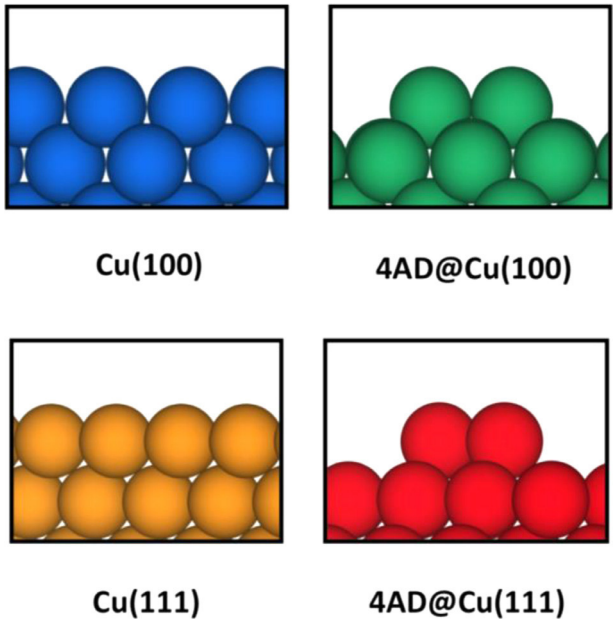

Fig. 1. Side views of the four different slab models used in this work. Top: Cu(100) (blue), 4AD@Cu(100) (green). Bottom: Cu(111) (orange), and 4AD@Cu(111) (red). Details on the number of atoms per layer and the number of layers in the slabs are provided in the Computational Methods section. (For interpretation of the references to color in this figure legend, the reader is referred to the web version of this article.)

2.2. Computational details

The DFT simulations were carried out using the VASP code [34] with the Perdew-Burke-Ernzerhof (PBE) exchange-correlation functional [35], and the PAW method [36]. To model Cu-poly and OD-Cu, we studied four different types of active sites: Cu(111) terraces; Cu(100) terraces; 4AD@Cu(100) and 4AD@Cu(111), which contain 4-atom islands on top of (100) and (111) terraces, respectively. A side view of the active sites is shown in Fig. 1. A $(4\sqrt{2} \times 4\sqrt{2})R45°$ supercell slab of 32 atoms per layer was used to model the Cu(100) and 4AD@Cu(100) surfaces. For Cu(111) and 4AD@Cu(111) a $p(4 \times 4)$ supercell including 16 atoms per layer was used. These large supercells help avoid lateral interactions between atom islands, adsorbates, and cations. All the slabs were modelled with the converged PBE lattice constant of Cu (3.64 Å) and were composed of four atomic layers. The adsorbates, Cu islands, and the top two layers of the slabs were allowed to relax in all directions, while the bottom layers were fixed at the bulk equilibrium distances. The plane-wave cutoff was 450 eV. The Methfessel-Paxton approach was used to smear the Fermi level with an electronic temperature of 0.2 eV, always extrapolating the total energies to 0 K. The numerical integration in the reciprocal space was carried out using Monkhorst-Pack grids of 2 × 2 × 1 for Cu(100) and 4AD@Cu(100) and 3 × 3 × 1 for Cu(111) and 4AD@Cu(111), which guaranteed convergence of the adsorption energies within ±0.05 eV. Periodically repeated images in the vertical direction were separated by more than 13 Å of vacuum and dipole corrections were also applied. The conjugate-gradient optimization algorithm was used for the geometry optimizations, with iterations performed until the maximal force on all atoms was below 0.05 eV $Å^{-1}$. Boxes of 9 × 10 × 11 $Å^3$ were used to calculate the isolated molecules in this study, considering the Γ-point only, using Gaussian smearing and an electronic temperature of 0.001 eV with further extrapolation to 0 K. On average, 10 different initial configurations were relaxed for each adsorbate on each active site,

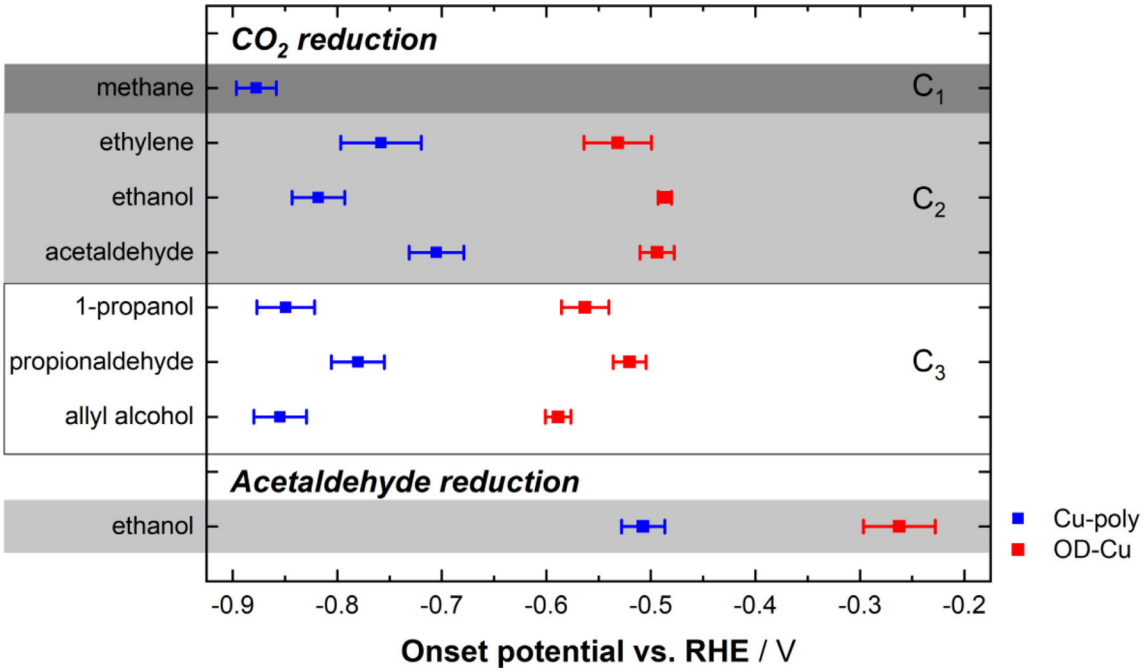

Fig. 2. Onset potentials of seven compounds from the reduction of CO_2, and onset of ethanol from the reduction of acetaldehyde. Error bars show the standard deviation of three independent measurements.

including, when possible, monodentate, bidentate, and tridentate configurations.

Reaction free energies were approximated as $\Delta G \approx \Delta E_{DFT} + \Delta ZPE - T\Delta S + \Delta E_{solvation}$, where ΔE_{DFT} is the DFT-calculated reaction energy, ΔZPE is the zero-point energy change, $T\Delta S$ is the corresponding entropy change at 298.15 K, and $\Delta E_{solvation}$ contains ad-hoc solvation corrections depending on the chemical nature of the adsorbates [14,25]. For free molecules, all contributions are considered in ΔS and the values were obtained from thermodynamic tables, while for adsorbates ΔS only includes the vibrational entropies. ZPE and TS_{vib} values are obtained from DFT calculations of vibrational frequencies making use of the harmonic-oscillator approximation.

Proton-electron pairs were modelled using the computational hydrogen electrode [37]. Cation effects were modelled by the explicit inclusion of a potassium atom over the slabs. In each case, we found around each adsorbate the most favorable position of the cation by relaxing different initial geometries. We did not compute proton-electron transfer barriers in this study, as Rossmeisl et al. recently noted that there is "not (yet) a method to obtain electrochemical barriers between realistic states at constant electrochemical conditions" [38]. Nevertheless, CO-CO coupling happens upon an electron transfer, so its barrier was assessed by means of the climbing-image nudged elastic band method [39], verifying that only one imaginary frequency along the reaction coordinate was present at the saddle point.

3. Results and discussion

We employed EC-RTMS together with linear sweep voltammetry to determine experimentally the onset potentials from the reduction of CO_2 for the following seven liquid and gaseous compounds: methane, ethylene, ethanol, acetaldehyde, 1-propanol, propionaldehyde and allyl alcohol. We also determined the onset potential for ethanol from the reduction of acetaldehyde. Fig. 2 shows the results for Cu-poly and OD-Cu electrodes, while a representative dataset can be found in the SI, Figure S2. All onset potentials are characterized by a small and constant standard deviation determined by three independent measurements, underlining the high reproducibility of the experiments.

On Cu-poly, methane shows the most negative onset potential with -0.88 ± 0.02 V_{RHE}. Different C_2 compounds (ethylene, ethanol) as well as C_3 compounds (1-propanol, propionaldehyde, allyl alcohol) show similarly negative onset potentials, ranging from -0.70 to -0.86 V_{RHE}, the least negative being the onset for acetaldehyde (-0.70 ± 0.03 V_{RHE}). Small deviations in these measurements might arise from different sensitivity of the instrumental method toward the detection of individual compounds. The fact that the experimental onset potentials are relatively similar for all C_{2+} products on Cu-poly suggests that their onset is controlled by a common potential-limiting step, early in the reaction pathway.

Interestingly, ethanol is produced from acetaldehyde reduction at a clearly less negative onset potential than from CO_2 (-0.51 ± 0.03 V_{RHE} versus -0.82 ± 0.03 V_{RHE}), which further supports that the onset potential for CO_2 reduction to ethanol through the acetaldehyde intermediate [13,40] is determined by another step, earlier in the reaction sequence, as shown by DFT-based models [14,16,25,41].

On OD-Cu, the onset potentials for all products of CO_2 reduction (except for methane, which is not detected) are shifted substantially to more positive values, spanning now from -0.49 ± 0.01 V_{RHE} for ethanol to -0.59 ± 0.02 V_{RHE} for allyl alcohol. As the onset potentials are similar among all C_{2+} products, we conclude that they likely still share a common potential-limiting step on OD-Cu, as is the case on Cu-poly. The onset potential for ethanol from the reduction of acetaldehyde shifts accordingly to more positive values (-0.27 ± 0.04 V_{RHE}) on OD-Cu, again more positive than from CO_2 on the same electrode, in line with the finding on Cu-poly. The significant shift of 250 mV on average for the onset potential of all reactions on OD-Cu compared to Cu-poly is ascribed to the creation of new active sites after the thermal treatment and subsequent oxide reduction [7–10,42,43]. We note that changes in the local pH or the local concentration of CO_2, which can be induced at the interface due to the higher roughness of OD-Cu and modify

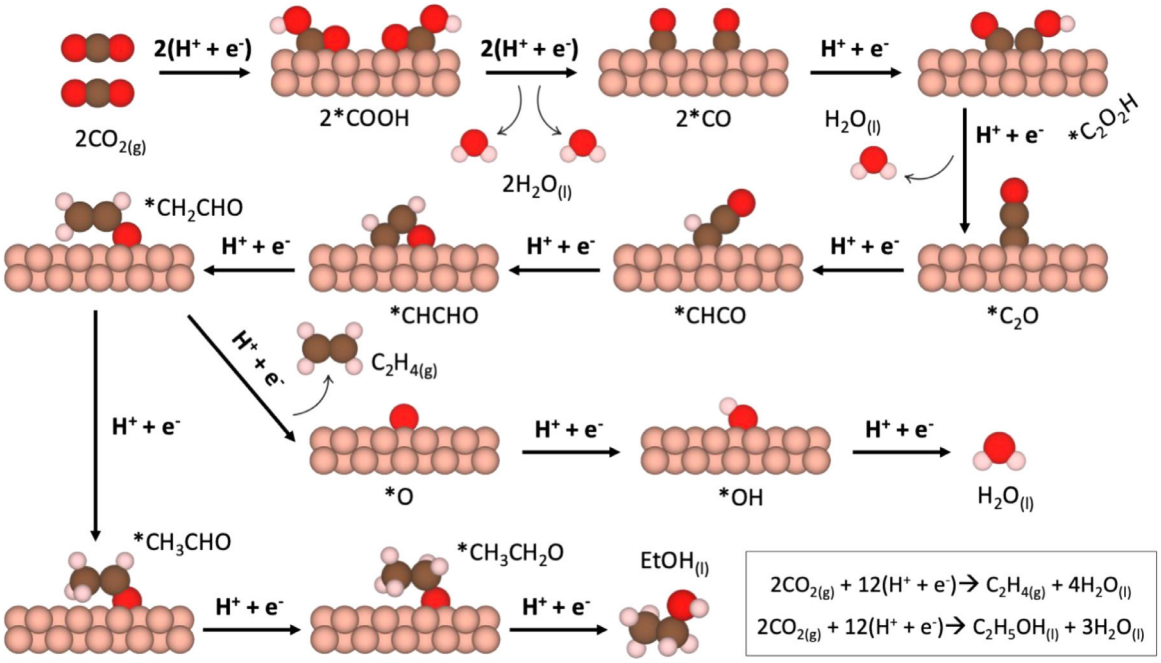

Fig. 3. Schematic representation of the reaction pathways for CO_2RR to C_2 species. Cu, C, O, and H atoms are depicted in grey, brown, red, and pink. EtOH: ethanol. (For interpretation of the references to color in this figure legend, the reader is referred to the web version of this article.)

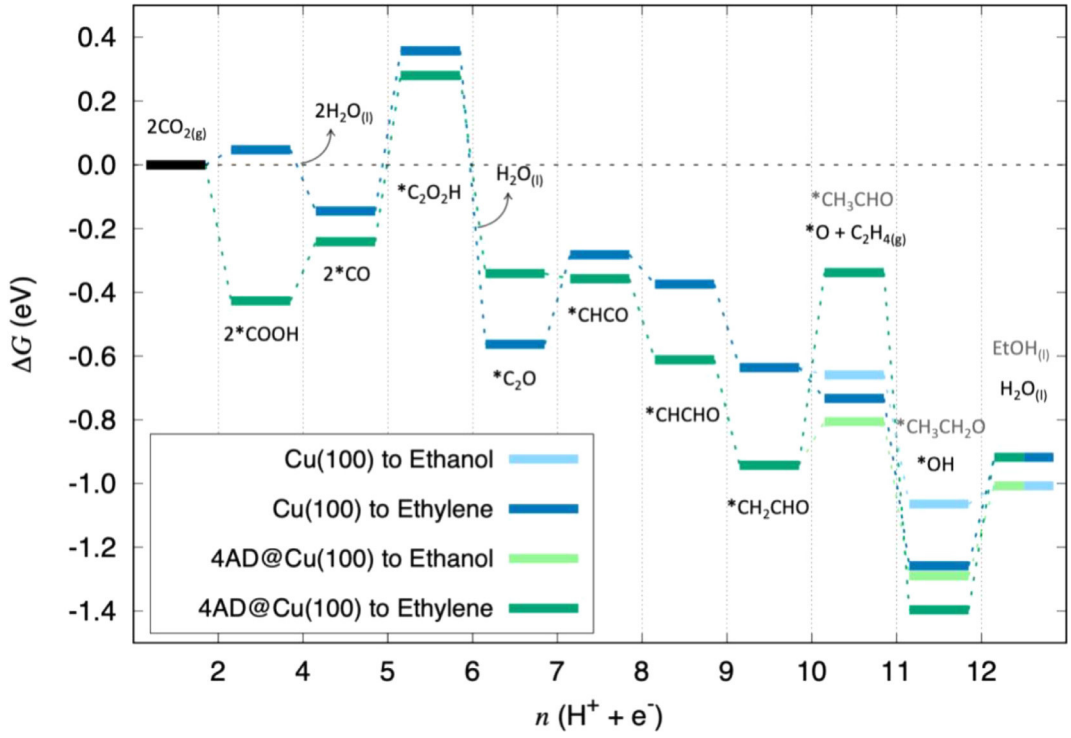

Fig. 4. Free-energy diagrams including solvent and cation effects for all intermediates of the CO_2RR to C_2 species on Cu(100) (blue) and 4AD@Cu(100) (green) at 0 V_{RHE}. The same colors in a lighter tone are used to represent the ethanol pathway, which drifts away from that of ethylene upon the tenth proton-electron transfer. The corresponding intermediates toward ethylene are noted for each proton-electron transfer in black (gray for the ethanol pathway). EtOH: Ethanol. (For interpretation of the references to color in this figure legend, the reader is referred to the web version of this article.)

the product distribution [44–47], are negligible here because the onsets were determined at rather low current densities and continuous electrolyte flow was employed.

Furthermore, the thermodynamics of each proton-electron transfer of CO_2RR to C_2 products (ethylene and ethanol) were calculated for four different active sites by combining well-known CO_2 reduction pathways to *CO via *COOH [27,48–51] with *CO reduction pathways that comply with several experimental observations [14,16,25]. The active sites selected for this study were Cu(111), as it is the most stable surface termination; Cu(100), known to facilitate C-C coupling and for being ethylene selective [14]; 4AD@Cu(100), a square, four-atom island likely present in

OD-Cu, the surface of which is extremely rough [52] and ethanol selective [16]; and, for completeness, 4AD@Cu(111), a four-atom island with hexagonal symmetry, which, as shown in previous works [16] and in Table S3, enhances CO dimerization with respect to Cu(111) but is not as active as the studied square sites, namely Cu(100) and 4AD@Cu(100).

A schematic representation of the modelled pathway is shown in Fig. 3. We find that the hydrogenation of adsorbed CO molecules ($2^*CO + H^+ + e^- \rightarrow {}^*C_2O_2H$) is the potential-limiting step of the reaction for ethylene and ethanol production on the analyzed active sites, in line with previous experimental and computational studies [6,14,53]. The fact that C-C coupling is involved in the potential-limiting step for C_2 products is also in agreement with the similar onset potentials determined experimentally with EC-RTMS for C_2 and C_3 products, bearing in mind that C_3 products are formed via a chemical reaction between C_1 and C_2 species [54–56]. We note here that $^*CO$ hydrogenation to either $^*COH$ or $^*CHO$ is also the potential-limiting step for CO_2RR to methane [17,24,27,57,58]. The onset potentials for CO_2RR to both ethylene and ethanol are −0.50, −0.52, −1.14, and −0.66 V_{RHE} for Cu(100), 4AD@Cu(100), Cu(111), and 4AD@Cu(111), respectively, calculated based on values from Table S3.

In Fig. 4, we show the calculated free-energy diagrams for these two surface models using the pathways in Fig. 3. After noting that (i) the calculated onset potentials for Cu(100) and 4AD@Cu(100) agree well with those determined experimentally for ethylene and ethanol on OD-Cu, and (ii) Cu(100) is selective to ethylene and 4AD@Cu(100) is selective to ethanol, we believe that the active sites present at OD-Cu responsible for ethylene and ethanol evolution resemble Cu(100) terraces and 4AD@Cu(100) islands, respectively. Cu(111) and 4AD@Cu(111) are not shown in Fig. 4 because they are not active toward C_2 products, given their unfavorable energetics of CO dimerization (see Table S3).

4. Conclusions

Because it is energy-intensive, the hydrogenation of $^*CO$ impedes an efficient CO_2 electroreduction. Hydrogenating $^*CO$ monomers is more difficult than hydrogenating $^*CO$ dimers on Cu electrodes. These two observations help explain why the onset potentials for all C_{2+} reaction products at a given electrode are similar and why more negative potentials are required for producing C_1 species compared to C_2 and C_3 species.

Furthermore, the notable differences in the experimental onset potentials between polycrystalline and oxide-derived copper electrodes, indicate the presence of a unique set of active sites in the latter. Based on DFT calculations affordably including solvent and cation effects, we propose that such sites are formed by square, four-atom ensembles of Cu atoms. Such configuration renders onset potentials for C_2 products that match the experimental values and complies with several experimental facts, namely that (i) oxide-derived Cu electrodes are extremely rough, (ii) square facets facilitate $^*CO$ coupling, and (iii) undercoordination favors ethanol production.

With all this in mind, we conclude that the selective production of a given multi-carbon product from CO_2RR requires not only engineering the C-C coupling step, which takes place early in the reaction mechanism, but also the bifurcation step, in which either the path toward oxygenates or hydrocarbons is followed.

Declaration of Competing Interest

The authors declare that they have no known competing financial interests or personal relationships that could have appeared to influence the work reported in this paper.

Credit authorship contribution statement

Oriol Piqué: Formal analysis, Investigation, Visualization, Writing – original draft. **Mario Löffler:** Formal analysis, Investigation, Visualization, Writing – original draft. **Ioannis Katsounaros:** Conceptualization, Formal analysis, Writing – review & editing, Supervision, Project administration. **Federico Calle-Vallejo:** Conceptualization, Formal analysis, Writing – review & editing, Supervision, Project administration, Funding acquisition.

Acknowledgments

F.C.-V. acknowledges funding from Spanish MICIUN RTI2018-095460-B-I00, Ramón y Cajal RyC-2015-18996 and María de Maeztu MDM-2017-0767 grants and partly by Generalitat de Catalunya 2017SGR13. O.P. thanks the Spanish MICIUN for a PhD grant (PRE2018-083811). We thank Red Española de Supercomputación (RES) for supercomputing time at SCAYLE (projects QS-2019-3-0018, QS-2019-2–0023, and QCM-2019-1-0034), MareNostrum (project QS-2020-1–0012), and CENITS (project QS-2020–2–0021). The use of supercomputing facilities at SURFsara was sponsored by NWO Physical Sciences, with financial support by NWO.

Supplementary materials

Supplementary material associated with this article can be found, in the online version, at doi:10.1016/j.electacta.2021.138247.

References

[1] S. Nitopi, E. Bertheussen, S.B. Scott, X. Liu, A.K. Engstfeld, S. Horch, B. Seger, I.E.L. Stephens, K. Chan, C. Hahn, J.K. Nørskov, T.F. Jaramillo, I. Chorkendorff, Progress and perspectives of electrochemical CO_2 reduction on copper in aqueous electrolyte, Chem. Rev. 119 (2019) 7610–7672, doi:10.1021/acs.chemrev.8b00705.

[2] O.S. Bushuyev, P.D. Luna, C.T. Dinh, L. Tao, G. Saur, J. van de Lagemaat, S.O. Kelley, E.H. Sargent, What should we make with CO_2 and how can we make it? Joule 2 (2018) 825–832, doi:10.1016/j.joule.2017.09.003.

[3] Y.Y. Birdja, E. Pérez-Gallent, M.C. Figueiredo, A.J. Göttle, F. Calle-Vallejo, M.T.M. Koper, Advances and challenges in understanding the electrocatalytic conversion of carbon dioxide to fuels, Nat. Energy 4 (2019) 732–745, doi:10.1038/s41560-019-0450-y.

[4] Y. Hori, A. Murata, R. Takahashi, S. Suzuki, Electroreduction of carbon monoxide to methane and ethylene at a copper electrode in aqueous solutions at ambient temperature and pressure, J. Am. Chem. Soc. 109 (1987) 5022–5023, doi:10.1021/ja00250a044.

[5] Y. Hori, A. Murata, R. Takahashi, Formation of hydrocarbons in the electrochemical reduction of carbon dioxide at a copper electrode in aqueous solution, J. Chem. Soc., Faraday Trans. 1. 85 (1989) 2309–2326, doi:10.1039/F19898502309.

[6] Y. Hori, R. Takahashi, Y. Yoshinami, A. Murata, Electrochemical reduction of CO at a copper electrode, J. Phys. Chem. B. 101 (1997) 7075–7081, doi:10.1021/jp970284i.

[7] C.W. Li, J. Ciston, M.W. Kanan, Electroreduction of carbon monoxide to liquid fuel on oxide-derived nanocrystalline copper, Nature 508 (2014) 504–507, doi:10.1038/nature13249.

[8] C.W. Li, M.W. Kanan, CO_2 reduction at low overpotential on Cu electrodes resulting from the reduction of thick Cu_2O films, J. Am. Chem. Soc. 134 (2012) 7231–7234, doi:10.1021/ja3010978.

[9] A. Verdaguer-Casadevall, C.W. Li, T.P. Johansson, S.B. Scott, J.T. McKeown, M. Kumar, I.E.L. Stephens, M.W. Kanan, I. Chorkendorff, Probing the active surface sites for CO reduction on oxide-derived copper electrocatalysts, J. Am. Chem. Soc. 137 (2015) 9808–9811, doi:10.1021/jacs.5b06227.

[10] Y. Lum, J.W. Ager, Evidence for product-specific active sites on oxide-derived Cu catalysts for electrochemical CO_2 reduction, Nature Catalysis 2 (2019) 86–93, doi:10.1038/s41929-018-0201-7.

[11] Y. Hori, I. Takahashi, O. Koga, N. Hoshi, Electrochemical reduction of carbon dioxide at various series of copper single crystal electrodes, J. Mol. Catal. A: Chem. 199 (2003) 39–47, doi:10.1016/S1381-1169(03)00016-5.

[12] P. Khanipour, M. Löffler, A.M. Reichert, F.T. Haase, K.J.J. Mayrhofer, I. Katsounaros, Electrochemical real-time mass spectrometry (EC-RTMS): monitoring electrochemical reaction products in real time, Angewandte Chemie International Edition 58 (2019) 7273–7277, doi:10.1002/anie.201901923.

[13] M. Löffler, P. Khanipour, N. Kulyk, K.J.J. Mayrhofer, I. Katsounaros, Insights into liquid product formation during carbon dioxide reduction on copper and oxide-derived copper from quantitative real-time measurements, ACS Catal. 10 (2020) 6735–6740, doi:10.1021/acscatal.0c01388.

[14] F. Calle-Vallejo, M.T.M. Koper, Theoretical considerations on the electroreduction of CO to C_2 species on Cu(100) electrodes, Angewandte Chemie International Edition 52 (2013) 7282–7285, doi:10.1002/anie.201301470.

[15] A. Rendón-Calle, S. Builes, F. Calle-Vallejo, A brief review of the computational modeling of CO_2 electroreduction on Cu electrodes, Curr. Opin. Electrochem. 9 (2018) 158–165, doi:10.1016/j.coelec.2018.03.012.

[16] O. Piqué, F. Viñes, F. Illas, F. Calle-Vallejo, Elucidating the structure of ethanol-producing active sites at oxide-derived Cu electrocatalysts, ACS Catal. 10 (2020) 10488–10494, doi:10.1021/acscatal.0c01880.

[17] J. Hussain, H. Jónsson, E. Skúlason, Calculations of product selectivity in electrochemical CO_2 reduction, ACS Catal. 8 (2018) 5240–5249, doi:10.1021/acscatal.7b03308.

[18] T. Cheng, H. Xiao, W.A. Goddard, Full atomistic reaction mechanism with kinetics for CO reduction on Cu(100) from ab initio molecular dynamics free-energy calculations at 298 K, PNAS (2017), doi:10.1073/pnas.1612106114.

[19] A. Murata, Y. Hori, Product selectivity affected by cationic species in electrochemical reduction of CO_2 and CO at a Cu electrode, BCSJ 64 (1991) 123–127, doi:10.1246/bcsj.64.123.

[20] J. Resasco, L.D. Chen, E. Clark, C. Tsai, C. Hahn, T.F. Jaramillo, K. Chan, A.T. Bell, Promoter effects of alkali metal cations on the electrochemical reduction of carbon dioxide, J. Am. Chem. Soc. 139 (2017) 11277–11287, doi:10.1021/jacs.7b06765.

[21] M.R. Singh, Y. Kwon, Y. Lum, J.W. Ager, A.T. Bell, Hydrolysis of electrolyte cations enhances the electrochemical reduction of CO_2 over Ag and Cu, J. Am. Chem. Soc. 138 (2016) 13006–13012, doi:10.1021/jacs.6b07612.

[22] E. Pérez-Gallent, G. Marcandalli, M.C. Figueiredo, F. Calle-Vallejo, M.T.M. Koper, Structure- and potential-dependent cation effects on CO reduction at copper single-crystal electrodes, J. Am. Chem. Soc. 139 (2017) 16412–16419, doi:10.1021/jacs.7b10142.

[23] Y. Basdogan, A.M. Maldonado, J.A. Keith, Advances and challenges in modeling solvated reaction mechanisms for renewable fuels and chemicals, WIREs Comput. Mol. Sci. 10 (2020) e1446, doi:10.1002/wcms.1446.

[24] A.A. Peterson, F. Abild-Pedersen, F. Studt, J. Rossmeisl, J.K. Nørskov, How copper catalyzes the electroreduction of carbon dioxide into hydrocarbon fuels, Energy Environ. Sci. 3 (2010) 1311–1315, doi:10.1039/C0EE00071J.

[25] S. Hanselman, M.T.M. Koper, F. Calle-Vallejo, Computational comparison of late transition metal (100) surfaces for the electrocatalytic reduction of CO to C_2 Species, ACS Energy Lett 3 (2018) 1062–1067, doi:10.1021/acsenergylett.8b00326.

[26] J.H. Montoya, C. Shi, K. Chan, J.K. Nørskov, Theoretical Insights into a CO Dimerization Mechanism in CO_2 Electroreduction, J. Phys. Chem. Lett. 6 (2015) 2032–2037, doi:10.1021/acs.jpclett.5b00722.

[27] A. Rendón-Calle, S. Builes, F. Calle-Vallejo, Substantial improvement of electrocatalytic predictions by systematic assessment of solvent effects on adsorption energies, Appl. Catal. B: Environ. (2020) 119147, doi:10.1016/j.apcatb.2020.119147.

[28] S.A. Akhade, W. Luo, X. Nie, A. Asthagiri, M.J. Janik, Theoretical insight on reactivity trends in CO_2 electroreduction across transition metals, Catal. Sci. Technol. 6 (2016) 1042–1053, doi:10.1039/C5CY01339A.

[29] L.D. Chen, M. Urushihara, K. Chan, J.K. Nørskov, Electric field effects in electrochemical CO_2 reduction, ACS Catal 6 (2016) 7133–7139, doi:10.1021/acscatal.6b02299.

[30] T. Ludwig, J.A. Gauthier, C.F. Dickens, K.S. Brown, S. Ringe, K. Chan, J.K. Nørskov, Atomistic insight into cation effects on binding energies in Cu-catalyzed carbon dioxide reduction, J. Phys. Chem. C. 124 (2020) 24765–24775, doi:10.1021/acs.jpcc.0c07004.

[31] S.A. Akhade, I.T. McCrum, M.J. Janik, The impact of specifically adsorbed ions on the copper-catalyzed electroreduction of CO_2, J. Electrochem. Soc. 163 (2016) F477, doi:10.1149/2.0581606jes.

[32] D. Bohra, J.H. Chaudhry, T. Burdyny, E.A. Pidko, W.A. Smith, Modeling the electrical double layer to understand the reaction environment in a CO_2 electrocatalytic system, Energy Environ. Sci. 12 (2019) 3380–3389, doi:10.1039/C9EE02485A.

[33] N. Martić, C. Reller, C. Macauley, M. Löffler, A.M. Reichert, T. Reichbauer, K.-.M. Vetter, B. Schmid, D. McLaughlin, P. Leidinger, D. Reinisch, C. Vogl, K.J.J. Mayrhofer, I. Katsounaros, G. Schmid, $Ag_2Cu_2O_3$ – a catalyst template material for selective electroreduction of CO to C_2+ products, Energy Environ. Sci. 13 (2020) 2993–3006, doi:10.1039/D0EE01100B.

[34] G. Kresse, J. Furthmüller, Efficient iterative schemes for ab initio total-energy calculations using a plane-wave basis set, Phys. Rev. B. 54 (1996) 11169–11186, doi:10.1103/PhysRevB.54.11169.

[35] J.P. Perdew, K. Burke, M. Ernzerhof, Generalized gradient approximation made simple, Phys. Rev. Lett. 77 (1996) 3865–3868, doi:10.1103/PhysRevLett.77.3865.

[36] G. Kresse, D. Joubert, From ultrasoft pseudopotentials to the projector augmented-wave method, Phys. Rev. B. 59 (1999) 1758–1775, doi:10.1103/PhysRevB.59.1758.

[37] J.K. Nørskov, J. Rossmeisl, A. Logadottir, L. Lindqvist, J.R. Kitchin, T. Bligaard, H. Jónsson, Origin of the overpotential for oxygen reduction at a fuel-cell cathode, J. Phys. Chem. B. 108 (2004) 17886–17892, doi:10.1021/jp047349j.

[38] A. Bagger, L. Arnarson, M.H. Hansen, E. Spohr, J. Rossmeisl, Electrochemical CO reduction: a property of the electrochemical interface, J. Am. Chem. Soc. 141 (2019) 1506–1514, doi:10.1021/jacs.8b08839.

[39] G. Henkelman, B.P. Uberuaga, H. Jónsson, A climbing image nudged elastic band method for finding saddle points and minimum energy paths, J. Chem. Phys. 113 (2000) 9901–9904, doi:10.1063/1.1329672.

[40] E. Bertheussen, A. Verdaguer-Casadevall, D. Ravasio, J.H. Montoya, D.B. Trimarco, C. Roy, S. Meier, J. Wendland, J.K. Nørskov, I.E.L. Stephens, I. Chorkendorff, Acetaldehyde as an intermediate in the electroreduction of carbon monoxide to ethanol on oxide-derived copper, Angewandte Chemie International Edition 55 (2016) 1450–1454, doi:10.1002/anie.201508851.

[41] I. Ledezma-Yanez, E.P. Gallent, M.T.M. Koper, F. Calle-Vallejo, Structure-sensitive electroreduction of acetaldehyde to ethanol on copper and its mechanistic implications for CO and CO_2 reduction, Catal Today 262 (2016) 90–94, doi:10.1016/j.cattod.2015.09.029.

[42] X. Feng, K. Jiang, S. Fan, M.W. Kanan, Grain-boundary-dependent CO_2 electroreduction activity, J. Am. Chem. Soc. 137 (2015) 4606–4609, doi:10.1021/ja5130513.

[43] R.G. Mariano, K. McKelvey, H.S. White, M.W. Kanan, Selective increase in CO_2 electroreduction activity at grain-boundary surface terminations, Science 358 (2017) 1187–1192, doi:10.1126/science.aao3691.

[44] M. Ma, K. Djanashvili, W.A. Smith, Controllable hydrocarbon formation from the electrochemical reduction of CO_2 over Cu nanowire arrays, Angewandte Chemie International Edition 55 (2016) 6680–6684, doi:10.1002/anie.201601282.

[45] Y. Lum, B. Yue, P. Lobaccaro, A.T. Bell, J.W. Ager, Optimizing C–C coupling on oxide-derived copper catalysts for electrochemical CO_2 reduction, J. Phys. Chem. C. 121 (2017) 14191–14203, doi:10.1021/acs.jpcc.7b03673.

[46] F.L.P. Veenstra, N. Ackerl, A.J. Martín, J. Pérez-Ramírez, Laser-microstructured copper reveals selectivity patterns in the electrocatalytic reduction of CO_2, Chem 6 (2020) 1707–1722, doi:10.1016/j.chempr.2020.04.001.

[47] H. Song, J.T. Song, B. Kim, Y.C. Tan, J. Oh, Activation of C_2H_4 reaction pathways in electrochemical CO_2 reduction under low CO_2 partial pressure, Appli. Catal. B: Environmental 272 (2020) 119049, doi:10.1016/j.apcatb.2020.119049.

[48] H.A. Hansen, J.B. Varley, A.A. Peterson, J.K. Nørskov, Understanding trends in the electrocatalytic activity of metals and enzymes for CO_2 reduction to CO, J. Phys. Chem. Lett. 4 (2013) 388–392, doi:10.1021/jz3021155.

[49] W. Zhu, Y.-J. Zhang, H. Zhang, H. Lv, Q. Li, R. Michalsky, A.A. Peterson, S. Sun, Active and selective conversion of CO_2 to CO on ultrathin Au nanowires, J. Am. Chem. Soc. 136 (2014) 16132–16135, doi:10.1021/ja5095099.

[50] J. Rosen, G.S. Hutchings, Q. Lu, S. Rivera, Y. Zhou, D.G. Vlachos, F. Jiao, Mechanistic insights into the electrochemical reduction of CO_2 to CO on nanostructured Ag surfaces, ACS Catal. 5 (2015) 4293–4299, doi:10.1021/acscatal.5b00840.

[51] L. Granda-Marulanda, A. Rendon-Calle, S. Builes, F. Illas, M.T.M. Koper, F. Calle-Vallejo, A semiempirical method to detect and correct DFT-based gas-phase errors and its application in electrocatalysis, ACS Catal 10 (2020) 6900–6907, doi:10.1021/acscatal.0c01075.

[52] M. Fields, X. Hong, J.K. Nørskov, K. Chan, Role of subsurface oxygen on Cu surfaces for CO_2 electrochemical reduction, J. Phys. Chem. C. 122 (2018) 16209–16215, doi:10.1021/acs.jpcc.8b04983.

[53] M. Gattrell, N. Gupta, A. Co, A review of the aqueous electrochemical reduction of CO_2 to hydrocarbons at copper, J. Electroanal. Chem. 594 (2006) 1–19, doi:10.1016/j.jelechem.2006.05.013.

[54] Y. Pang, J. Li, Z. Wang, C.-.S. Tan, P.-.L. Hsieh, T.-.T. Zhuang, Z.-.Q. Liang, C. Zou, X. Wang, P. De Luna, J.P. Edwards, Y. Xu, F. Li, C.-.T. Dinh, M. Zhong, Y. Lou, D. Wu, L.-.J. Chen, E.H. Sargent, D. Sinton, Efficient electrocatalytic conversion of carbon monoxide to propanol using fragmented copper, Nat. Catal. 2 (2019) 251–258, doi:10.1038/s41929-019-0225-7.

[55] R. Kortlever, J. Shen, K.J.P. Schouten, F. Calle-Vallejo, M.T.M. Koper, Catalysts and reaction pathways for the electrochemical reduction of carbon dioxide, J. Phys. Chem. Lett. 6 (2015) 4073–4082, doi:10.1021/acs.jpclett.5b01559.

[56] X. Chang, A. Malkani, X. Yang, B. Xu, Mechanistic insights into electroreductive C–C coupling between CO and Acetaldehyde into multicarbon products, J. Am. Chem. Soc. 142 (2020) 2975–2983, doi:10.1021/jacs.9b11817.

[57] X. Nie, M.R. Esopi, M.J. Janik, A. Asthagiri, Selectivity of CO_2 reduction on copper electrodes: the role of the kinetics of elementary steps, Angewandte Chemie International Edition 52 (2013) 2459–2462, doi:10.1002/anie.201208320.

[58] F. Calle-Vallejo, M.T.M. Koper, Accounting for bifurcating pathways in the screening for CO_2 reduction catalysts, ACS Catal 7 (2017) 7346–7351, doi:10.1021/acscatal.7b02917.

Supporting Information

Computational-Experimental Study of the Onset Potentials for CO_2 reduction on Polycrystalline and Oxide-Derived Copper Electrodes

Oriol Piqué,[1] Mario Löffler,[2,3] Ioannis Katsounaros,[2,*] and Federico Calle-Vallejo[1,*]

[1] Department of Materials Science and Physical Chemistry & Institute of Theoretical and Computational Chemistry (IQTCUB), University of Barcelona, Martí i Franquès 1, 08028 Barcelona, Spain.

[2] Helmholtz Institute Erlangen-Nürnberg for Renewable Energy (IEK-11), Forschungszentrum Jülich GmbH, Egerlandstr. 3, 91058 Erlangen, Germany.

[3] Department of Chemical and Biological Engineering, Friedrich-Alexander-Universität Erlangen-Nürnberg (FAU), Egerlandstr. 3, 91058 Erlangen, Germany

*Emails: i.katsounaros@fz-juelich.de, f.calle.vallejo@ub.edu

Table of contents

S1 Onset potential determination from mass ion signals

In electrochemical real-time mass spectrometry, mass ion signals are recorded as a response to an electrochemical excitation. Let us assume that such an electrochemical excitation leads to the occurrence of a reaction and the formation of a product at time $t = t_0$. As a result, the mass ion signal for that product rises from the background at a time $t = t_0 + \Delta t$. The finite response time Δt is caused by the transport of the product together with the electrolyte from the cell to the mass spectrometer through the tubings and the respective inlet system for each setup. The response time Δt can be determined from electrochemical pulse experiments by subtracting the time stamps of the electrochemical excitation and the mass spectrometer signature.

Moreover, when no electrochemical reaction takes place, the mean (μ) and standard deviation (σ) of the recorded background signal in the mass spectrometer are defined. We calculated the μ and σ from at least 100 data points, to have sufficient statistics as illustrated in Figure S1 over 50 seconds. If now, as depicted in Figure S1, a linear sweep voltammogram starts from a potential E_{start} (-0.4 V_{RHE} in the figure) at $t = t_0 = 0$, the mass spectrometer signal rises to $\mu+\sigma$ at time $t = \Delta t + t_1$, where t_1 is the time needed to reach the potential E_{onset} where the product is detected. Clark and Bell use the one-sigma level as "detection limit" [1]. The one-sigma level above the mean background signal ensures that natural fluctuations in the mass spectrometer signal are cancelled out. Knowing the t_1, the E_{onset} can be calculated using the sweep rate, υ, from the equation: $E_{onset} = E_{start} - t_1 \upsilon$, for a negative-going scan. The potential applied vs the Ag/AgCl reference electrode is calculated vs the reversible hydrogen electrode and post-corrected for the *iR* drop according to a previously described procedure [2].

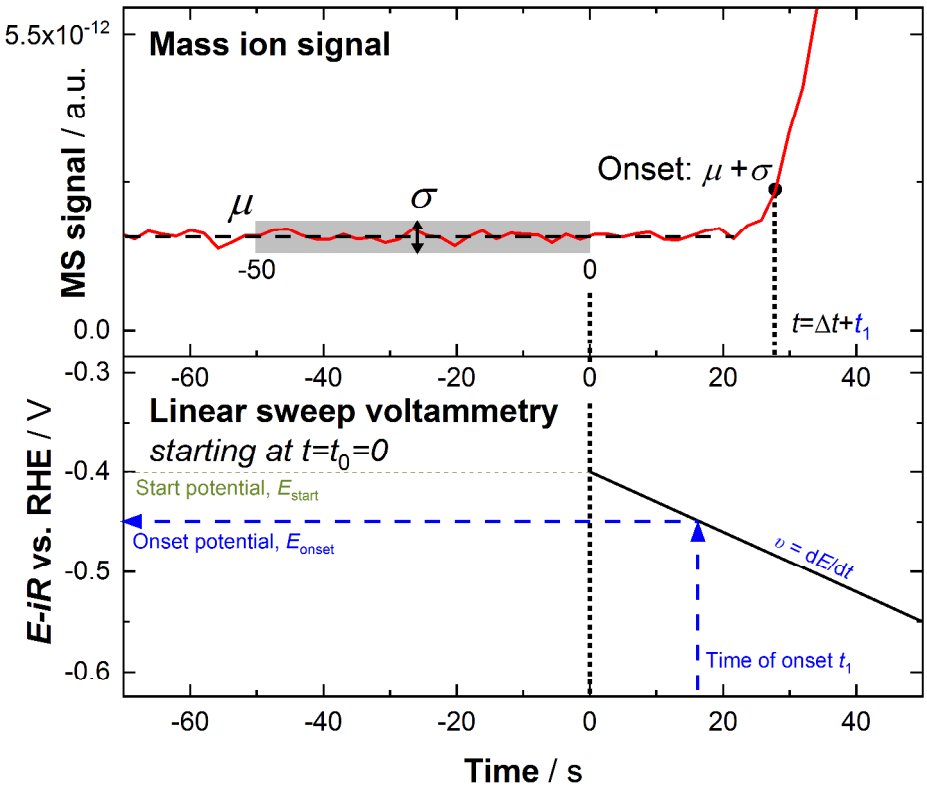

Figure S1. Determination of the onset potential from mass spectrometer signals resulting from the application of linear sweep voltammetry.

S2 Representative linear sweep voltammetry measurements

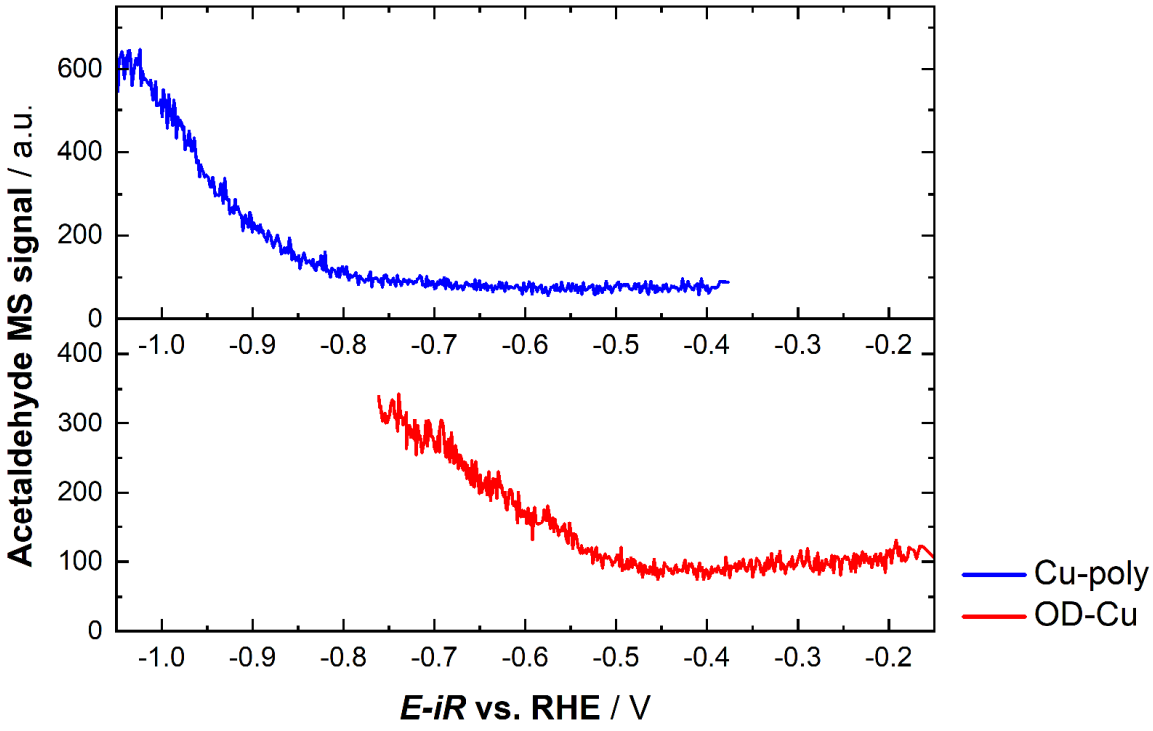

Figure S2. Representative linear sweep voltammetry measurements and mass spectrometry signals for acetaldehyde on polycrystalline (blue) and oxide-derived (red) copper.

S3 Gaseous phase corrections

The free energies of gaseous molecules were calculated as: $G \approx E_{DFT} + ZPE - TS$. The ZPE values were obtained from vibrational frequency analyses. The TS values were extracted from thermodynamic tables at 298.15 K and 1 atm [3]. The values used for all of the gases featured in this study are listed in Table S1. Because the PBE exchange-correlation functional does not describe correctly the free energy of $CO_{(g)}$ and $CO_{2(g)}$, corrections to their formation energies of -0.24 eV and 0.19 eV were applied, respectively, which are in line with those obtained in previous studies [4],[5],[6].

Table S1. Zero-point energy and entropy contributions to the free energies of gaseous molecules. All values are in eV.

Molecule	ZPE	TS
CO_2	0.31	0.66
CO	0.14	0.61
H_2	0.27	0.40
C_2H_4	1.36	0.68
H_2O	0.57	0.58
CH_3CHO	1.47	0.82
C_2H_5OH	2.11	0.87

S4 Liquid-phase corrections

For the products present in the liquid phase (namely water, ethanol, and acetaldehyde), the free energies were estimated using the method described in ref. [4], which is based on a correction added to the TS values. Specifically, TS values of 0.67 eV, 0.94 eV, and 0.87 eV were used to estimate the liquid-phase free energies of water, ethanol, and acetaldehyde, respectively.

S5 Solvation contributions to the free energies

Water-adsorbate interactions, deemed "solvation" corrections (E_{sol} in $G \approx E_{DFT} + ZPE - TS + E_{sol}$) were modeled as an external, ad hoc correction depending on the chemical nature of the adsorbates. We used the values reported in previous works [4,7]. The specific values used are listed in Table S2. These were obtained by calculating the difference in adsorption energies with and without water, using √3×√3 Cu(111) cells covered with and without water and *OH, *COH, and *CO. The *OR correction was

approximated as 2/3 of that for *ROH, since, in principle, *ROH can make three hydrogen bonds with water (two accepting, two donating bonds), while *OR can only make two (two accepting bonds). Note that R represents a hydrocarbon chain. Values in Table S2 are commensurate with those in the literature [5,8].

Table S2. Stabilization provided by water-adsorbate interactions to the adsorption energies depending on the adsorbates' chemical structure. All values are given in eV.

Functional group	Solvation Correction
*CO	-0.10
*OH	-0.50
*ROH	-0.38
*OR	-0.25

S6 Adsorption energies

The respective ZPE, TS_{vib}, and solvation (E_{sol}) corrections, and ΔG values obtained for the different adsorbates featured in this study are a combination of data from previous works [7] and new calculations performed in this one. All the data are listed in Table S3. The most stable configuration (MSC) for each adsorbate is also indicated. $*C_2O_2H$ and *COOH are particular cases in which one part of the adsorbate interacts with the K atom and a solvation correction for the other group is included. Liquid acetaldehyde was considered when it was more stable than its adsorbed counterpart. Note that $2CO_{2(g)}$ and proton-electron pairs were used as the reference for the free energies in Table S3.

Table S3. Free energies of adsorption and their separate contributions for each species involved in CO_2 electroreduction to C_2 species. All values are in eV.

Cu(100)	ZPE	TS_{vib}	MSC	ΔG
2 *COOH	1.22	0.48	K + Solvated (-0.38)	0.05
2 *CO	0.36	0.33	With K	-0.15
$*C_2O_2H$	0.69	0.26	K + Solvated (-0.38)	0.36
$*C_2O$	0.34	0.19	With K	-0.56
*CHCO	0.60	0.24	With K	-0.28
*CHCHO	0.91	0.17	With K	-0.37
$*CH_2CHO$	1.21	0.20	Solvated (-0.25)	-0.64
$*CH_3CHO$	1.47	0.87	Liquid	-0.66
$*CH_3CH_2O$	1.83	0.30	Solvated (-0.25)	-1.06
*O	0.06	0.05	With K	-0.73
*OH	0.34	0.10	Solvated (-0.50)	-0.92

4AD@Cu(100)	ZPE	TS_{vib}	MSC	ΔG
2 *COOH	1.24	0.44	K + Solvated (-0.38)	-0.43
2 *CO	0.37	0.38	Solvated (-0.20)	-0.24
*C_2O_2H	0.70	0.26	K + Solvated (-0.38)	0.28
*C_2O	0.33	0.19	Solvated (-0.10)	-0.34
*CHCO	0.60	0.24	Solvated (-0.10)	-0.36
*CHCHO	0.90	0.17	Solvated (-0.25)	-0.61
*CH_2CHO	1.21	0.20	With K	-0.94
*CH_3CHO	1.48	0.32	Solvated (-0.25)	-0.81
*CH_3CH_2O	1.83	0.30	With K	-1.29
*O	0.06	0.05	With K	-0.34
*OH	0.35	0.09	Solvated (-0.50)	-1.40

Cu(111)	ZPE	TS_{vib}	MSC	ΔG
2 *COOH	1.22	0.46	K + Solvated (-0.38)	0.22
2 *CO	0.35	0.36	With K	0.02
*C_2O_2H	0.71	0.31	K + Solvated (-0.38)	1.16
*C_2O	0.34	0.19	With K	-0.04
*CHCO	0.60	0.24	With K	0.06
*CHCHO	0.90	0.18	With K	-0.02
*CH_2CHO	1.19	0.20	With K	-0.36
*CH_3CHO	1.47	0.87	Liquid	-0.66
*CH_3CH_2O	1.84	0.31	Solvated (-0.25)	-0.83
*O	0.07	0.04	With K	-0.32
*OH	0.34	0.08	Solvated (-0.50)	-0.96

4AD@Cu(111)	ZPE	TS_{vib}	MSC	ΔG
2 *COOH	1.24	0.44	K + Solvated (-0.38)	-0.59
2 *CO	0.37	0.40	Solvated (-0.20)	-0.41
*C_2O_2H	0.71	0.25	K + Solvated (-0.38)	0.24
*C_2O	0.34	0.19	With K	-0.40
*CHCO	0.61	0.23	Solvated (-0.10)	-0.45
*CHCHO	0.90	0.18	With K	-0.75
*CH_2CHO	1.21	0.25	With K	-1.17
*CH_3CHO	1.48	0.26	Solvated (-0.25)	-0.84
*CH_3CH_2O	1.84	0.32	Solvated (-0.25)	-1.28
*O	0.07	0.04	With K	-0.59
*OH	0.34	0.09	Solvated (-0.50)	-1.44

References

[1] E.L. Clark, A.T. Bell, Direct Observation of the Local Reaction Environment during the Electrochemical Reduction of CO2, J. Am. Chem. Soc. 140 (2018) 7012–7020. https://doi.org/10.1021/jacs.8b04058.

[2] M. Löffler, P. Khanipour, N. Kulyk, K.J.J. Mayrhofer, I. Katsounaros, Insights into Liquid Product Formation during Carbon Dioxide Reduction on Copper and Oxide-Derived Copper from Quantitative Real-Time Measurements, ACS Catal. 10 (2020)

6735–6740. https://doi.org/10.1021/acscatal.0c01388.

[3] D.R. Lide, CRC Handbook of Chemistry and Physics, 85th ed., CRC Press, Boca Raton, FL, 2005.

[4] F. Calle□Vallejo, M.T.M. Koper, Theoretical Considerations on the Electroreduction of CO to C2 Species on Cu(100) Electrodes, Angewandte Chemie International Edition. 52 (2013) 7282–7285. https://doi.org/10.1002/anie.201301470.

[5] A.A. Peterson, F. Abild-Pedersen, F. Studt, J. Rossmeisl, J.K. Nørskov, How copper catalyzes the electroreduction of carbon dioxide into hydrocarbon fuels, Energy Environ. Sci. 3 (2010) 1311–1315. https://doi.org/10.1039/C0EE00071J.

[6] R. Christensen, H. A. Hansen, T. Vegge, Identifying systematic DFT errors in catalytic reactions, Catalysis Science & Technology. 5 (2015) 4946–4949. https://doi.org/10.1039/C5CY01332A.

[7] O. Piqué, F. Viñes, F. Illas, F. Calle-Vallejo, Elucidating the Structure of Ethanol-Producing Active Sites at Oxide-Derived Cu Electrocatalysts, ACS Catal. 10 (2020) 10488–10494. https://doi.org/10.1021/acscatal.0c01880.

[8] A. Rendón-Calle, S. Builes, F. Calle-Vallejo, Substantial improvement of electrocatalytic predictions by systematic assessment of solvent effects on adsorption energies, Applied Catalysis B: Environmental. (2020) 119147. https://doi.org/10.1016/j.apcatb.2020.119147.